IEEE Access
Multidisciplinary ⋮ Rapid Review ⋮ Open Access Journal

Received June 10, 2021, accepted June 25, 2021, date of publication July 5, 2021, date of current version July 14, 2021.

Digital Object Identifier 10.1109/ACCESS.2021.3094772

Multi-Receiver Cross-Correlation Technique for (B)FSK Radios

VIJAYA KUMAR PURUSHOTHAMAN[1], (Student Member, IEEE), MINA R. M. MIKHAEL[2], MARK S. OUDE ALINK[1], (Senior Member, IEEE), ERIC A. M. KLUMPERINK[1], (Fellow, IEEE), ANDRÉ B. J. KOKKELER[3], (Member, IEEE), AND BRAM NAUTA[1], (Fellow, IEEE)

[1]IC-Design Group, Faculty of Electrical Engineering, Mathematics and Computer Science, University of Twente, 7522 NB Enschede, The Netherlands
[2]ItoM B. V., 5624 CL Eindhoven, The Netherlands
[3]Radio Systems Group, Faculty of Electrical Engineering, Mathematics and Computer Science, University of Twente, 7522 NB Enschede, The Netherlands

Corresponding author: Vijaya Kumar Purushothaman (v.k.purushothaman@utwente.nl)

This work was supported by the Netherlands Organisation for Scientific Research (NWO), through TTW-Research Program under Project 13576 IRUDIT.

ABSTRACT This article presents a multi-receiver cross-correlation technique for (B)FSK receivers, targeting wireless sensor network applications. Here, multiple receiver outputs are pair-wise cross-correlated and the correlated output samples are averaged to lower the noise floor at the receiver output. Compared to a two-receiver cross-correlation, multi-receiver cross-correlation generates more cross-correlated output samples in a given time. Hence it requires a shorter measurement time for a desired noise floor reduction and facilitates a higher data rate for (B)FSK operation. Compared to a single receiver, it improves the linearity and the harmonic interferer tolerance using passive splitters and different LO frequencies in the receiver paths respectively. These theoretical insights are verified with measurements for the first time using a 2- and 3-receiver cross-correlation in a BFSK receiver. Operating at 1 GHz and with a data rate of 200 kbps, the demonstrator, using sub-mW mixer-first receiver front-ends for power efficiency, achieves −102 dBm sensitivity and >40 dB rejection for both narrow and wideband harmonic interferers without any RF filters.

INDEX TERMS Cross-correlation, mixer-first receiver, passive mixer, BFSK, noise reduction, low power, interferer-robustness, harmonic rejection, wireless sensor network.

I. INTRODUCTION

Cross-correlation (XC) can be used as an energy detection technique that mitigates noise uncertainty in spectrum-sensing CMOS receivers, targeting cognitive radio applications [1]–[4]. In this technique, the outputs of two receivers, receiving the same RF input, are cross-correlated with each other, as shown in Fig. 1. When a large number of cross-correlated output samples is averaged, the uncorrelated noise contributions of the two receivers average out to zero, leaving the correlated signal with a lower noise floor at the correlator output. Thus, the effective Signal-to-Noise Ratio (SNR) improves after XC and facilitates signal detection even in a low-SNR environment. Additionally, passive attenuators can be used at the receiver input to improve its linearity and dynamic range, as the resulting noise can be recovered using XC [2], [5]. Despite the increased power consumption, XC is an attractive option to improve the receiver performance in scenarios where circuit techniques "*hit the SNR wall* [6]," owing to its orthogonality to those techniques [5].

Recently, we proposed to use XC for data-communication in receivers targeting wireless sensor networks [7], [8]. Among digital modulation schemes, Frequency Shift Keying (FSK) is chosen as it can be demodulated using the energy detection principle in the frequency discriminator [8], [9]. As seen in Fig. 2, the received Binary-FSK (BFSK) signals can be demodulated non-coherently by detecting and comparing the signal power in the frequency bins corresponding to transmitted '0'/'1' binary data. Such signal detection in FSK discriminators can be improved through XC technique. We demonstrated this in [7], [8] through theoretical calculations and MATLAB simulations.

The SNR improvement due to XC, in general, increases with the number of cross-correlated output samples averaged at the expense of measurement time [2]. Since the measurement time in BFSK receivers is constrained by its data rate, the SNR increment due to XC is limited [7].

The associate editor coordinating the review of this manuscript and approving it for publication was Mauro Fadda.

To overcome this trade-off, we proposed 'multi-receiver XC' that uses more than two receiver paths (or simply '2-paths') to generate more cross-correlated output samples in a given time [4], [8]. The effect of multi-receiver XC on the bit error rate of BFSK receivers is mathematically analysed in [8], but without experimental verification. In this work, we implemented the multi-receiver XC technique in a BFSK receiver using state-of-the-art sub-mW front-end, designed for IoT applications [10] and evaluated experimentally the improvement in sensitivity and harmonic interferer tolerance of the receiver. We also show that multi-receiver XC consumes less energy to generate the same number of useful cross-power spectrum samples than a two-path XC. Besides FSK receivers, the proposed multi-receiver XC can be used in applications such as dynamic spectrum sensing, direction finding, and radio-interferometry [2]–[4], [11].

The article is organized as follows. Section II discusses the multi-receiver XC technique and its application to BFSK receivers. Section III describes the experimental set-up used for multi-receiver XC, while Section IV presents the measurement results. Finally, conclusions are presented in Section V.

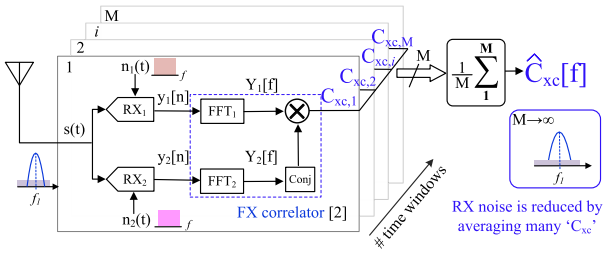

FIGURE 1. A 2-path cross-correlation technique [2] using *'M'* time-windows to generate *'M'* correlated output samples.

II. MULTI-RECEIVER CROSS-CORRELATION

A cross-power spectrum, C_{xc}, contains both the correlated signal-and-noise and uncorrelated noise contributions of the two receivers. It has been shown that averaging 'M' C_{xc} samples reduces the uncorrelated noise power at the correlator output asymptotically by a factor of $1/\sqrt{M}$ [1]. This means the XC improves the SNR by about 1.5 dB when the number of averaged C_{xc} samples is doubled. As shown in Fig. 1, the C_{xc} samples are generated by repeatedly applying the time-windowed FX-correlator [1] on the incoming receiver signals at the expense of longer measurement time and narrower bandwidth and hence, lower date [2], [3], [7]. For example, reference [2] reported about 12 dB improvement in the SNR at the output of a 2-path cross-correlated receiver by increasing the measurement time by a factor of 273 ($273 \approx 2^8$; $8 \times 1.5 = 12$ dB).

Alternatively in [8], we increased the number of cross-power spectrum samples by increasing the number of receivers used in the XC, as shown in Fig. 3. When 'k' ($k > 1$) receivers are pair-wise cross-correlated simultaneously, $\binom{k}{2}$ cross-correlated output samples are available in a single time-window. In this way, more cross-power spectrum samples are generated without compromising on measurement time and thereby enabling increased data-rate operation in (B)FSK receivers. To understand the power-efficiency of multi-receiver XC, let us assume each receiver, FFT, conjugate-multiplication, and averaging operation consumes a power of P_{RX}, P_{FFT}, P_{MAC}, and P_A respectively. The total power consumption in a 'k'-receiver path XC can be given as,

$$P_{XC,k} = k\,(P_{RX} + P_{FFT}) + \binom{k}{2} P_{MAC} + P_A \qquad (1)$$

Often, receivers and FFTs consume significantly more power than other digital circuits in typical XC receivers [2], [3], [5], [8]. Hence, we assume here that $P_{RX} + P_{FFT} \gg P_{MAC} + P_A$. For small k, this simplifies (1) into

$$P_{XC,k} \approx k\,(P_{RX} + P_{FFT}) = kP_{avg,1} \qquad (2)$$

where $P_{avg,1} \triangleq P_{RX} + P_{FFT}$ is the average power consumed in single receiver path in multi-receiver XC implementation. The average power spent to generate one C_{xc} sample is

$$P_{XC,avg} \simeq \frac{kP_{avg,1}}{\binom{k}{2}} = \frac{2P_{avg,1}}{k-1} \qquad (3)$$

As the number of receiver paths, k, increases, the average power spent to produce one C_{xc} sample reduces (Fig. 4). Hence, for more C_{xc} samples, it is more energy efficient to increase the number of receiver paths in the XC than increasing the number of time-windows of an FX-correlator in a 2-path XC, provided the C_{xc} samples are sufficiently uncorrelated [8].

In a BFSK receiver, XC reduces the required SNR at the output of each receiver to demodulate with a certain bit error rate (BER), assumed in this paper to be 10^{-3} [7]. Using the mathematical model developed in [8], the SNR benefit of multi-receiver XC in a BFSK system was estimated. Simulated results are presented in Fig. 5, where the noise in the receiver paths is assumed to be fully uncorrelated. As shown in the figure, increasing the number of receiver paths and/or time-windows in the FX-correlator will reduce

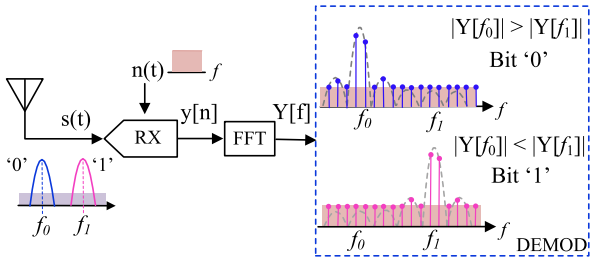

FIGURE 2. A typical non-coherent BFSK receiver using an FFT-based demodulator.

[1] In an FX-correlator, the input samples are frequency transformed (F) before conjugate multiplication (X). It is the other way around in an XF-correlator [2].

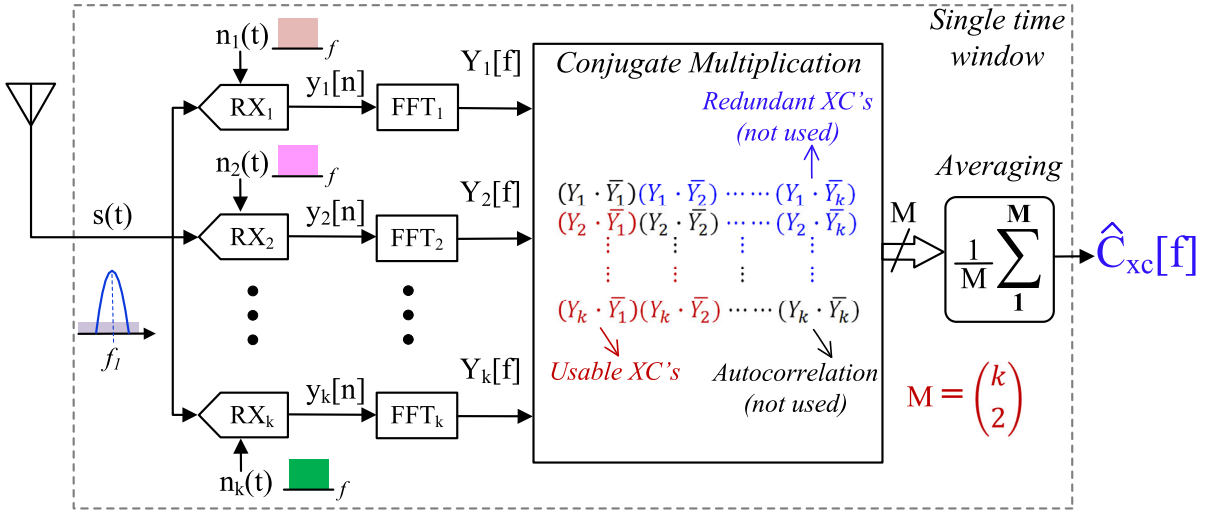

FIGURE 3. An overview of a multi-receiver cross-correlation technique.

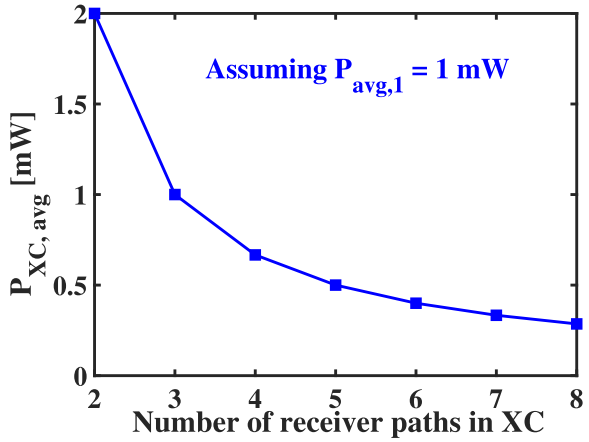

FIGURE 4. Average power consumption for one C_{xc} sample vs. number of receiver paths in XC, calculated using (3).

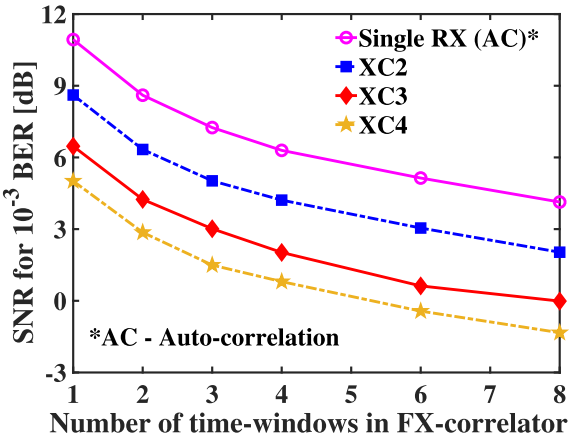

FIGURE 5. Required SNR at the output of each receiver for BFSK demodulation with 10^{-3} BER vs. the number of time-windows used in FX-correlator based on simulations.

the required SNR for BFSK demodulation. By generating more C_{xc} samples per time-window, 3-path and 4-path XCs use fewer time-windows to achieve the desired SNR performance than 2-path XC. For a more detailed analysis on the influence of multi-receiver XC on BFSK receivers, readers are kindly referred to our previous work [8].

The SNR improvement with XC could degrade because of signal decorrelation and noise correlation in the receiver paths [1], [4]. The correlated noise in the receiver paths defines the minimum achievable noise floor at the XC output. Hence receivers should be sufficiently isolated from each other to reduce their noise correlation and sufficiently identical to reduce signal decorrelation [2], [8].

III. CROSS-CORRELATION BASED BFSK RECEIVER SET-UP

We will first experimentally verify the benefit of using 2-path XC in a BFSK receiver and then the effect of using multi-receiver XC technique.

The experimental set-up used for this demonstration is shown in Fig. 7. The RF input is fed into multiple receiver paths using power splitters, instead of using resistive dividers as in [2]. Power splitters are preferred here for following reasons. First, low-power passive mixer-first receiver front-ends are used here for XC. Since they have no reverse isolation, the passive mixer-first front-ends require isolators at its inputs to reduce noise correlation. The resistive dividers provide limited isolation between the front-ends connected to their output terminals [5]. Hence, using resistive dividers would increase the correlated noise floor at the output of the front-ends and degrades the noise figure post-XC. Resistive dividers also prohibit the use of distinct LO frequencies in the mixer-first front-ends and thus no harmonic rejection improvement [5]. Hence, off-chip power splitters are used here for isolating mixer-first front-ends. By providing 50 Ω impedance at its output terminals, power splitters also

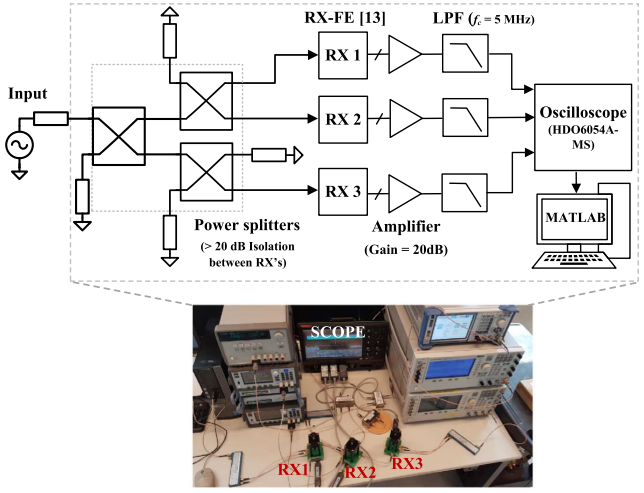

FIGURE 6. Experimental set-up of a 3-receiver XC based BFSK receiver.

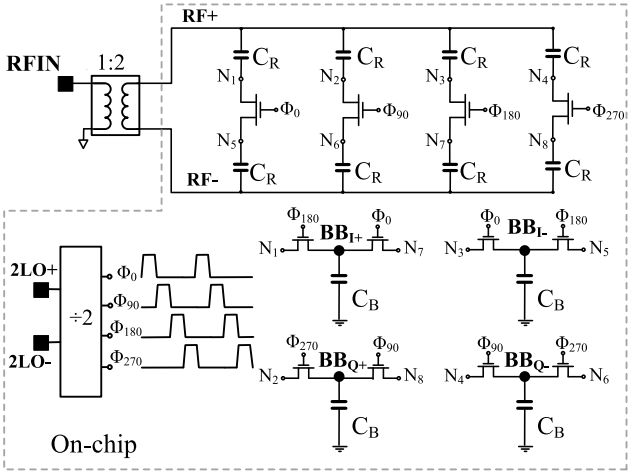

FIGURE 7. A fully-passive sub-mW mixer-first receiver front-end [10].

facilitate impedance matching at the input of mixer-first front-ends [10]. Please note that the power splitters can be avoided if receivers with high input impedance are used for XC, instead of mixer-first front-ends [5]. Each splitter in the multi-receiver XC technique provides an insertion loss of ∼1 dB and 20 dB isolation between its output ports. Since the input signal splits evenly between its output ports, each splitter provides 4 dB loss (3 dB + 1 dB insertion loss) in the signal path. This translates to 8 dB attenuation in each receiver path in this demonstrator. Such signal attenuation lowers the distortion components in the receiver and makes the receiver more interferer-robust, while noise can be recovered by multi-receiver XC. As such, multi-receiver XC improves the overall dynamic range of the receiver [2], [5].

Behind the splitters, each path uses a mixer-first receiver front-end that we proposed in [10]. As shown in Fig 7, the front-end employs a 4-path differential bottom-plate filter/mixer with RF capacitors (C_R) and baseband capacitors (C_B) and an off-chip step-up transformer [10]. The filtered RF voltage in the differential 4-path filter is sensed from the bottom-plate terminals N_{1-8} of the C_R capacitors for down-conversion. Thanks to implicit capacitive stacking, this results in a passive voltage gain of 6 dB at the baseband output [10]. Implemented in a 22 nm CMOS FDSOI process, this fully-passive RF front-end achieves 14 dB V-V gain, 5 dB NF, and +25 dBm IIP3 while consuming only 0.6 mW at 1 GHz LO frequency. Such low power consumption is the reason for using this front-end in this multi-receiver XC demonstrator.

The I/Q baseband outputs from the front-end are 20 dB amplified by an external amplifier (LeCroy AP033). It is followed by a passive low-pass filter with 5 MHz bandwidth for anti-aliasing. An oscilloscope (Teledyne HDO6054A-MS) with built-in ADCs is used to convert the baseband signals into digital outputs. Implemented in MATLAB, the DSP comprises FX-correlators and an FSK demodulator. FX-correlators are used here for their low implementation complexity, compared to XF-correlators [2]. The demodulator compares the energy in the relevant frequency bins of the cross-power spectrum to decode the input data.

Each receiver path from power splitter to ADC provides 34 dB voltage gain and exhibits an output noise floor with a power spectral density of −130 dBm/Hz, shown in Fig. 8. With 8 dB splitter loss, this translates to a ∼14 dB noise figure for each individual receiver. Thanks to >20 dB isolation, noise correlation between the receivers can be approximated as $1/F$, where F is the noise factor of a single receiver (Appendix A). Since each receiver path exhibits 14 dB noise figure, this translates to a noise correlation ratio of ∼0.04. Such noise correlation would limit the reduction in the required SNR at the output of each receiver for 10^{-3} BER to 2.6 / 4.4 / 5.4 dB for single time-windowed 2 / 3 / 4-path XCs, respectively [7, Fig.6]. Since the additional SNR improvement is only 1 dB between 3-path and 4-path XC, the 3-path XC is chosen here as an optimum in the trade-off between SNR improvement and power consumption.

IV. MEASUREMENT RESULTS AND DISCUSSION

The insertion loss of cables is de-embedded from all the measurement results, while that of the splitters remains included. All receivers use an LO frequency of 1 GHz unless specified otherwise. In all measurements, both the auto-correlator (for single RX) and the FX-correlator are operated for only one time-window to keep the measurement time as short as possible. This results in one and three C_{xc} samples from 2-path and 3-path XC, respectively.

A. SENSITIVITY PERFORMANCE

A BFSK signal with a data rate of 200 kbps and a frequency spacing of 400 kHz is applied at the input. It is modulated at a carrier frequency of 1.003 GHz so that the down-converted IF at 3 MHz will not be influenced by the flicker noise of the baseband amplifiers (Fig. 8). Sensitivity, defined as the input power for which the receiver achieves a 10^{-3} BER, is measured for three different scenarios and the results obtained are

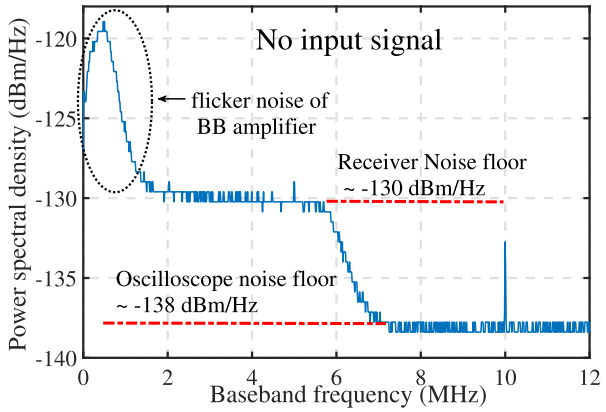

FIGURE 8. Measured power spectral density at the ADC output with no RF input.

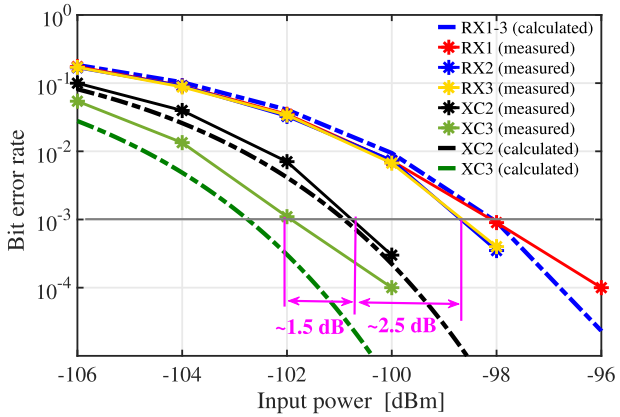

FIGURE 9. Measured and calculated BER vs input power for individual receivers (RX1, RX2, RX3), 2-path XC (XC2), and 3-path XC (XC3).

presented in Fig. 9. In the first scenario, where receivers with splitters are individually measured, all 3 receivers achieve a sensitivity of −98.0 dBm through autocorrelation. In the second scenario, when two receivers are cross-correlated (XC2), the system achieves a sensitivity of −100.5 dBm, showing an expected 2.5 dB improvement compared to a single RX with the same single time-window operation. The calculated and measured BER is shown in the figure for comparison. The measured BER results are within a 0.5 dB margin of the calculated values, respectively, see Section II. In the third scenario, where 3-path XC (XC3) is used, an additional 2 dB improvement in sensitivity is expected based on the calculations for single time-window operation. Accordingly, the measurement reports a −102.0 dBm sensitivity, a 1.5 dB and 4.0 dB improvement compared to XC2 and a single receiver, respectively. Thus in a low-SNR environment, multi-receiver XC provides the flexibility to combine multiple receiver outputs for better signal detection.

B. HARMONIC REJECTION PERFORMANCE

Using different LO frequencies in each receiver path, XC has shown to improve the harmonic rejection

TABLE 1. Input and output spectrum of 3 BFSK receivers for harmonic rejection measurement.

Receivers	RX1	RX2	RX3	Units
Input Signal ($f_{\mathrm{RF,w}}$)	1004	1004	1004	MHz
Interferer ($f_{\mathrm{RF,int}}$)	3004	3004	3004	MHz
Local Oscillator (f_{LO})	999	1000	1001	MHz
$f_{\mathrm{IF,w}}$ ($f_{\mathrm{RF,w}} - f_{\mathrm{LO}}$)	5	4	3	MHz
$f_{\mathrm{IF,int}}$ ($f_{\mathrm{RF,int}} - 3f_{\mathrm{LO}}$)	7	4	1	MHz

performance [12], [13]. To evaluate this benefit here, a BFSK signal ($f_{\mathrm{RF,w}}$) at a carrier frequency of 1004 MHz and a −50 dBm sinusoidal interferer ($f_{\mathrm{RF,int}}$) at 3004 MHz are applied at the receiver input. The LO frequencies of the receivers are chosen such that the interferer coincides with the desired BFSK signal in one of the paths after down-conversion, as indicated in Table 1. The frequency offsets between the receiver outputs due to different LOs are corrected before XC in the digital domain [13]. For the given LO frequency selection, RX1 and RX3 are less affected by 3rd harmonic mixing, whereas RX2 deteriorates drastically since the interferer falls exactly on the desired signal after down-conversion with a 1000 MHz LO. As shown in Fig. 10, RX1 and RX3 achieve a reduced sensitivity of −93 dBm due to limited interferer rejection at its baseband, whereas RX2 fails, even upto an input power of −83 dBm. When the RX2 output is cross-correlated with other receivers, the harmonic interferer tolerance improves significantly. The receiver achieves a sensitivity of −88 dBm and −92 dBm with 2-path and 3-path XC, respectively, even in the

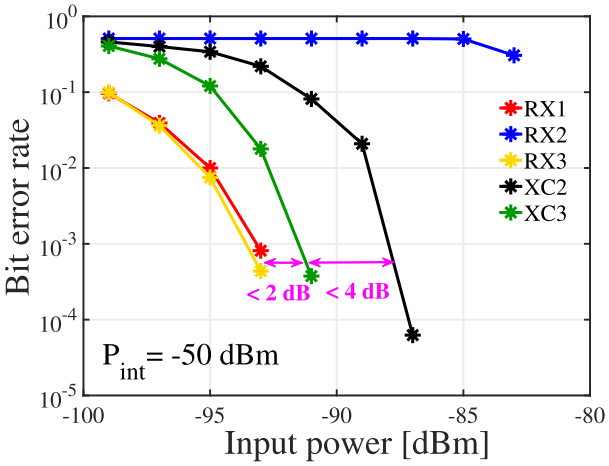

FIGURE 10. Measured sensitivity at f_{LO} = 1 GHz of the RX1, RX2, RX3, XC2, and XC3 in the presence of a 3rd harmonic sinusoid interferer at 3004 MHz with P_{int} = −50 dBm.

presence of a −50 dBm harmonic interferer. Using 3-path XC, the receiver can tolerate a >40 dB stronger harmonic unmodulated interferer.

The degradation due to a narrow-band harmonic interferer can be overcome by using only the uncorrupted receivers (RX1 / RX3). However, it is difficult to identify the uncorrupted receivers without prior knowledge of the received data. Further, if the interferer is wideband with time-varying center frequency, then using the "*best available RX*" is not an optimal solution. This is because each frequency bin, corresponding to the desired input, in all three receivers can be corrupted, at least in part, by harmonic interferers. Thanks to different LO frequencies, the interferer contributions in these frequency bins remain uncorrelated. Hence, when these corrupted frequency bins are cross-correlated, the uncorrelated interferer content in those bins will be averaged out, similar to noise in those frequency bins. To verify this feature, a −50 dBm QPSK-modulated interferer with 8 MHz bandwidth, centered at 3 GHz, is applied at the receiver input. LO and the input signal frequencies remain unchanged compared to the previous scenario. The 8 MHz BW is sufficient to corrupt the desired signal for all the three receivers after down-conversion. Similar to earlier scenarios, the sensitivity of individual receivers, XC2, and XC3 are measured and presented in Fig. 11. As seen in the figure, XC2 and XC3 achieve 3 dB and 7 dB better sensitivity than the individual receivers, similar to the improvement in Fig. 9 for noise. This validates the benefit of XC in the scenarios with uncertain and wideband interferers.

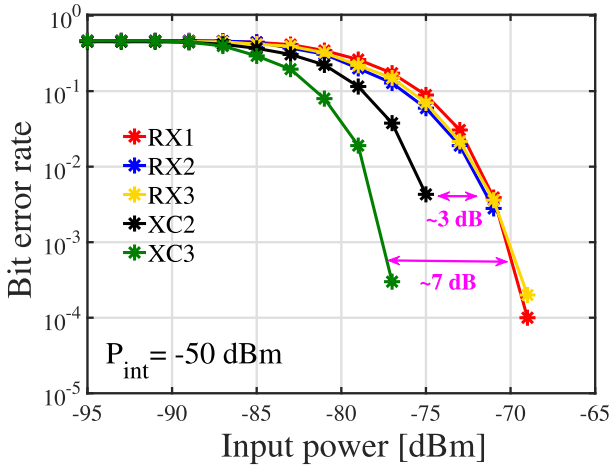

FIGURE 11. Measured sensitivity with and without cross-correlation in the presence of a QPSK interferer at 3 GHz with $P_{int} = -50$ dBm.

C. DISCUSSION

The experimental results in this section validate the benefits of the XC technique in BFSK receivers. Using 3-receiver XC, a 200 kbps BFSK receiver reduces its noise floor at the output of the FX-correlator by 4 dB and tolerates a 40 dB stronger harmonic interferer at no expense of measurement time, as in [2]. However, such improvement comes at the cost of power and area due to multiple receiver paths and DSP blocks. Implementing the DSP in an advanced CMOS process with optimal number of bits and FFT points [2], [8] and using low-power receivers [14] would lower the power consumption significantly. On-chip power splitters and oscillator pulling [15] might provide a challenge that should be further explored for realizing single chip implementation of multi-receiver XC. Though power splitters degrade the noise figure of the receiver, precisely 8 dB, it improves the linearity and harmonic interferer tolerance of the receiver considerably. Since 3-path XC partially compensates the noise degradation (4 dB), the overall dynamic range of the receiver is improved in this implementation. As such, XC allows for the possibility of a flexible receiver-cluster that could achieve better reception in a crowded low-SINR environment than the individual receivers. In better SNR scenarios, the XC can be switched off and the receivers can be untethered either for individual reception or turned off to save power.

V. CONCLUSION

This article demonstrates the application of XC in BFSK receivers. XC using two receivers lowers the required SNR at each receiver output for BFSK demodulation at the expense of measurement time and power. Multi-receiver XC reduces this measurement time by doing pair-wise XC of multiple receiver outputs concurrently, while consuming less energy than a 2-path XC for given detection performance. Using distinct LO frequencies in each receiver path, the multi-receiver XC can tolerate large narrow and wideband harmonic interferers. This is demonstrated using a 3-path XC based BFSK receiver with state-of-the-art 22 nm FDSOI front-ends. A 4 dB noise floor reduction at the receiver output and a −92 dBm BFSK signal reception in the presence of −50 dBm harmonic interferer (both narrow band and wideband) are verified. In summary, XC technique seems a viable option for achieving interferer-robustness in low-power receivers.

APPENDIX A
RELATIONSHIP BETWEEN THE NOISE CORRELATION COEFFICIENT AND THE NOISE FACTOR

Let us first define the noise parameters before calculating noise correlation coefficient, ρ.

- n_x is a random variable representing the circularly symmetric complex Gaussian (CSCG) noise that is added to all the receiver paths at the input as a shared noise, where $n_x \sim \mathcal{CN}(0, \sigma_x^2)$ [8];
- $n_{c,i}$ is a random variable representing CSCG noise added only to the i^{th} receiver path, where $n_{c,i} \sim \mathcal{CN}(0, \sigma_c^2)$;
- Noise added in the receiver paths are considered to be uncorrelated with each other. Hence, their covariance, $\text{Cov}(n_{c,i_1}, n_{c,i_2}) = 0, \forall i_1 \neq i_2$;
- The shared noise and the receiver noise are assumed to be uncorrelated with each other. So, $\text{Cov}\left(n_x, n_{c,i}\right) = 0, \forall i$;

- $n_{t,i}$ represents the total noise in the i^{th} receiver path: $n_{t,i} = n_x + n_{c,i}$. Thus, $n_{t,i} \sim \mathcal{CN}(0, \sigma_n^2)$ where $\sigma_n^2 = \sigma_x^2 + \sigma_c^2$.

The noise correlation, ρ_{i_1,i_2} between the total noise in the receiver paths, i_1 and i_2 for $i_1 \neq i_2$ can be given as

$$\rho_{i_1,i_2} \triangleq \frac{\text{Cov}(n_{t,i_1}, n_{t,i_2})}{\sqrt{\text{Var}(n_{t,i_1})\text{Var}(n_{t,i_2})}} = \frac{\text{E}((n_x + n_{c,i_1})(n_x + n_{c,i_2})^*)}{\sqrt{(\sigma_n^2)(\sigma_n^2)}} = \frac{\sigma_x^2}{\sigma_n^2},$$

where * denotes complex conjugation. Since ρ_{i_1,i_2} is identical for all pairs, we can write $\rho_{i_1,i_2} = \rho, \forall i_1 \neq i_2$.

The noise factor is defined as the SNR at the system input (the shared noise) divided by the SNR at the system output (total noise):

$$F \triangleq \frac{\text{SNR}_\text{i}}{\text{SNR}_\text{o}} = \frac{1/\sigma_x^2}{1/\sigma_n^2} = \frac{\sigma_n^2}{\sigma_x^2} = \frac{1}{\rho}.$$

REFERENCES

[1] M. S. Oude Alink, "RF spectrum sensing in CMOS exploiting cross correlation," Ph.D. dissertation, Univ. Twente, Enschede, The Netherlands, 2013.

[2] M. S. Oude Alink, E. A. M. Klumperink, A. B. J. Kokkeler, M. C. M. Soer, G. J. M. Smit, and B. Nauta, "A CMOS-compatible spectrum analyzer for cognitive radio exploiting crosscorrelation to improve linearity and noise performance," *IEEE Trans. Circuits Syst. I, Reg. Papers*, vol. 59, no. 3, pp. 479–492, Mar. 2012.

[3] M. Kitsunezuka and K. S. J. Pister, "Cross-correlation-based, phase-domain spectrum sensing with low-cost software-defined radio receivers," *IEEE Trans. Signal Process.*, vol. 63, no. 8, pp. 2033–2048, Apr. 2015.

[4] J. C. Merritt and J. D. Chisum, "High-speed cross-correlation for spectrum sensing and direction finding of time-varying signals," *IEEE Sensors J.*, vol. 18, no. 15, pp. 6161–6168, Aug. 2018.

[5] M. S. Oude Alink, E. A. M. Klumperink, A. B. J. Kokkeler, Z. Ru, W. Cheng, and B. Nauta, "Using crosscorrelation to mitigate analog/RF impairments for integrated spectrum analyzers," *IEEE Trans. Microw. Theory Techn.*, vol. 61, no. 3, pp. 1327–1337, Mar. 2013.

[6] M. S. Oude Alink, A. B. J. Kokkeler, E. A. M. Klumperink, G. J. M. Smit, and B. Nauta, "Lowering the SNR wall for energy detection using cross-correlation," *IEEE Trans. Veh. Technol.*, vol. 60, no. 8, pp. 3748–3757, Oct. 2011.

[7] M. R. M. Mikhael, M. S. Oude Alink, and A. B. J. Kokkeler, "A cross-correlation sub-sampling receiver for low power applications in a low SINR environment," in *Proc. IEEE 9th Annu. Inf. Technol., Electron. Mobile Commun. Conf. (IEMCON)*, Nov. 2018, pp. 1108–1112.

[8] M. R. M. Mikhael, M. S. Oude Alink, and A. B. J. Kokkeler, "Using multiple chains in cross-correlation receivers to improve sensitivity," in *Proc. IEEE 90th Veh. Technol. Conf. (VTC-Fall)*, Sep. 2019, pp. 1–7.

[9] S. Haykin and M. Moher, *Communication Systems*, 4th ed. Hoboken, NJ, USA: Wiley, 2010.

[10] V. K. Purushothaman, E. A. M. Klumperink, B. T. Clavera, and B. Nauta, "A fully passive RF front end with 13-dB gain exploiting implicit capacitive stacking in a bottom-plate N-path filter/mixer," *IEEE J. Solid-State Circuits*, vol. 55, no. 5, pp. 1139–1150, May 2020.

[11] E. Ryman, A. Emrich, S. B. Andersson, L. Svensson, and P. Larsson-Edefors, "1.6 GHz low-power cross-correlator system enabling geostationary Earth orbit aperture synthesis," *IEEE J. Solid-State Circuits*, vol. 49, no. 11, pp. 2720–2729, Nov. 2014.

[12] N. A. Moseley, E. A. M. Klumperink, and B. Nauta, "A spectrum sensing technique for cognitive radios in the presence of harmonic images," in *Proc. 3rd IEEE Symp. New Frontiers Dyn. Spectr. Access Netw.*, Oct. 2008, pp. 1–10.

[13] M. S. Oude Alink, A. B. J. Kokkeler, E. A. M. Klumperink, Z. Ru, W. Cheng, and B. Nauta, "Improving harmonic rejection for spectrum sensing using crosscorrelation," in *Proc. ESSCIRC (ESSCIRC)*, Sep. 2012, pp. 361–364.

[14] D. D. Wentzloff, A. Alghaihab, and J. Im, "Ultra-low power receivers for IoT applications: A review," in *Proc. IEEE Custom Integr. Circuits Conf. (CICC)*, Mar. 2020, pp. 1–8.

[15] T.-H. Lee, *The Design of CMOS Radio-frequency Integrated Circuits*, 2nd ed. Cambridge, U.K.: Cambridge Univ. Press, 2004.

VIJAYA KUMAR PURUSHOTHAMAN (Student Member, IEEE) received the bachelor's degree in electronics and communication from the College of Engineering, Guindy, Chennai, India, in 2011, and the M.Sc. degree in electrical engineering (microelectronics) from the Delft University of Technology, Delft, The Netherlands, in 2016. He is currently pursuing the Ph.D. degree with the Integrated Circuit Design Group, University of Twente, Enschede, The Netherlands. From 2011 to 2013, he was with Synopsys Inc., Bangalore, India, working as an Application Engineer. His research interest includes analog and radio-frequency circuits and systems for low-power interferer-robust transceivers.

MINA R. M. MIKHAEL received the B.Sc. degree in electrical engineering from Ain Shams University, in 2011, and the M.Sc. degree in electrical engineering from Nile University, in 2015. He is currently pursuing the Ph.D. degree with the University of Twente. In 2019, he joined ItoM, where he is working on digital PLLs, CDRs, and demodulators. His research interest includes low-power interference-robust receivers.

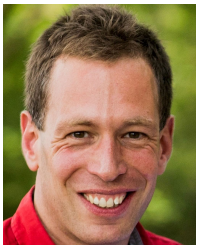

MARK S. OUDE ALINK (Senior Member, IEEE) was born in Hengelo, The Netherlands, in 1984. He received the joint M.Sc. degrees *(cum laude)* in electrical engineering and computer science, in 2008, and the Ph.D. degree *(cum laude)* from the University of Twente, Enschede, The Netherlands, in 2013. After several years in industry as a system engineer and a RFIC design engineer, he returned to his alma mater as an Assistant Professor with the IC-Design Group. His research interests include low-power and digitally-assisted analog and RF circuits and systems. He has been serving on the Technical Program Committee of the Custom Integrated Circuits Conference (CICC), since 2018. He was a recipient of the Prestigious Else Kooi Award. He has been a Guest Editor of the CICC 2020 and 2021 Special Issues in the IEEE JOURNAL OF SOLID-STATE CIRCUITS.

ERIC A. M. KLUMPERINK (Fellow, IEEE) was born in Lichtenvoorde, The Netherlands, in 1960. He received the B.Sc. degree from HTS, Enschede, in 1982. He worked in industry on digital hardware and software. In 1984, he joined the University of Twente, Enschede, shifting focus to analog CMOS circuit research. This resulted in several publications and his Ph.D. thesis "Transconductance Based CMOS Circuits: Circuit Generation, Classification and Analysis," in 1997. In 1998, he started as an Assistant Professor with the IC-Design Laboratory, University of Twente, and shifted research focus to RF CMOS circuits (e.g., sabbatical at Ruhr Universitaet, Bochum, Germany). Since 2006, he has been as an Associate Professor, a Teaching Analog and RF IC Electronics, and a Guiding Ph.D. and M.Sc. projects related to RF CMOS circuit design with focus on software defined radio, cognitive radio, and beamforming. He holds several patents, authored, and coauthored more than 175 internationally refereed journal articles and conference papers. He has been a member of the technical program committee of IEEE RFIC Symposium, since 2011. He was recognized as more than 20 ISSCC paper contributors, from 1954 to 2013. He was a co-recipient of the ISSCC 2002 and the ISSCC 2009 Van Vessem Outstanding Paper Award. He served as an Associate Editor for the IEEE Transactions on Circuits and Systems—II: Express Briefs, from 2006 to 2007, IEEE Transactions on Circuits and Systems—I: Regular Papers, from 2008 to 2009, and the IEEE Journal of Solid-State Circuits, from 2010 to 2014, an IEEE SSC Distinguished Lecturer, from 2014 to 2015, and a member of the technical program committees of ISSCC, from 2011 to 2016.

ANDRÉ B. J. KOKKELER (Member, IEEE) received the Ph.D. degree from the University of Twente, in 2005. He has worked more than six years at Ericsson as a System Engineer and eight years at the Netherlands Foundation for Research in Astronomy (ASTRON) as a Scientific Project Manager. He is currently appointed as an Associate Professor with the University of Twente. He has a background in telecommunication, mixed signal design, and signal processing architectures. He is involved in research projects, sponsored by the Dutch and European governments and industry. His current research interest includes design of low-power architectures for telecommunications and computationally intensive applications. His research focuses on efficient realization of digital signal processing for communications.

BRAM NAUTA (Fellow, IEEE) was born in Hengelo, The Netherlands, in 1964. He received the M.Sc. degree *(cum laude)* in electrical engineering and the Ph.D. degree from the University of Twente, in 1987 and 1991, respectively, on the subject of analog CMOS filters for very high frequencies. In 1991, he joined the Mixed-Signal Circuits and Systems Department, Philips Research, Eindhoven, The Netherlands. In 1998, he returned to the University of Twente, where he is currently a Distinguished Professor with the IC Design Group. Since 2016, he has been serving as the Chair of the Electrical Engineering Department, University of Twente. His current research interests include high-speed analog CMOS circuits, software defined radio, cognitive radio, and beamforming. He is a member of the Royal Netherlands Academy of Arts and Sciences (KNAW). He was in the Technical Program Committee of the Symposium on VLSI Circuits, from 2009 to 2013. He is in the Steering Committee and Programme Committee of the European Solid State Circuit Conference (ESSCIRC). He was a co-recipient of the ISSCC 2002 and 2009 "Van Vessem Outstanding Paper Award."In 2014, he received the 'Simon Stevin Meester' Award (500.000 €) and the largest Dutch national prize for achievements in technical sciences. He served as the Editor-in-Chief for the IEEE Journal of Solid-State Circuits (JSSC), from 2007 to 2010, and an Associate Editor for IEEE Transactions on Circuits and Systems—II: Express Briefs, from 1997 to 1999, and IEEE Journal of Solid-State Circuits, from 2001 to 2006. He was the Program Chair of the International Solid State Circuits Conference (ISSCC), in 2013, and the President of the IEEE Solid-State Circuits Society, from 2018 to 2019. He served as a Distinguished Lecturer for the IEEE.